DESIGN AND DEVELOPMENT OF DELTA WING WITH LOITERING CAPABILITY

Shannon Yip Ying En, Kwan Qiao Le, Akhilesh Karthikeyan, Benedict Goh Yong En
Victoria Junior College, 20 Marine Vista, Singapore 449035
Nanyang Girls' High School, 2 Linden Dr, Singapore 288683
Anderson-Serangoon Junior College, 1033 Upper Serangoon Road, Singapore 534768
National Junior College, 37 Hillcrest Road, Singapore 288913
Mentors: Lim Zhi Wei Jonathan, Wong Jun Han Amos Timothy
DSO National Laboratories

Abstract

The aim of this study is to capitalise on the strong Leading-Edge Vortices (LEVs) that are characteristic of delta wings, and adapt designs based on current research such that it would be most suited for low-loitering flights. Three variables, sweep angle, airfoil thickness, and the addition of wing fences, were analysed at subsonic conditions. The team designed a prototype using *SolidWorks* and modified the design to study the effects of the factors mentioned. Based on results collected using Computational Fluid Dynamics (CFD), the wing with 45° sweep angle and NACA 2408 airfoil was the most optimal, maximising range and endurance. While reducing airfoil thickness (NACA2404) and adding wing fences enhanced LEVs generation, it came at the cost of increased C_D, limiting endurance and range. Nonetheless, our research underscores the potential of delta wings in the realm of low-loitering flights. Addressing the primary challenge of minimising C_D in the new delta wing design, further geometric optimization of wing fences emerges as a promising avenue, potentially leading to improved endurance and range and, consequently, heightened low-loitering capabilities.

Nomenclature

C_D – Drag coefficient
C_L – Lift coefficient
α – Angle of attack
L/D ratio – Lift to drag ratio

Introduction

In recent years, a surge in natural disasters, conflicts, and humanitarian crises has underscored the need for enhanced capabilities in reconnaissance, surveillance or search and rescue [1]. Regarding this, one commonly employed tool is low-loitering drones, which provides the capacity to hold and release necessary resources, while moving slowly enough for necessary information to be captured. Not only are these drones much more affordable than building conventional large scale planes, they are also much more adaptable. For example, after Turkey was struck by a 7.8 magnitude earthquake in February 2023, traditional aircraft faced operational challenges due to adverse weather conditions. In contrast, the Bayraktar Akıncı low-loitering Unmanned Combat Aerial Vehicles (UCAVs) proved resilient, conducting successful flights in unfavourable weather. The low-loitering flight allowed onboard cameras to clearly capture ground activity, providing valuable insights into the disaster's meteorological aspects. This aided the crisis response team in damage detection, search and rescue, and overall coordination efforts

highlighting the effectiveness of unmanned aerial vehicles in enhancing disaster response capabilities.

Low-loitering planes can be equipped with many types of wings. However, in such missions, split second decisions often have to be made, such as making sharp turns to rescue victims or even speeding up to avoid detection. In this, Delta wings, known for their stability, agility and responsiveness [2] in low-loitering scenarios where precise and adaptable flight control is vital, is a more practical option.

In the case of maximising the capabilities of low-loitering flight, our criteria would be to maximise the range and endurance such that the aircraft is able to efficiently utilise fuel while minimising excessive drag contributing to improved flight duration.

This means maximising the lift coefficient, C_L, to increase duration which the plane is able to fly, and minimising the drag coefficient, C_D, which allows an aircraft to have greater range and endurance [3]. Assuming constant velocity, pressure and rate of fuel burn, we use the Breguet

Endurance equation: $E = \frac{\eta_p}{\gamma_p}\sqrt{2\rho S}\frac{{C_L}^{1.5}}{C_D}\left(\frac{1}{\sqrt{W_1}} - \frac{1}{\sqrt{W_2}}\right)$, (constant ρ, α) [4]

and Range Equation: $R = \frac{\eta_p}{\gamma_p}\frac{C_L}{C_D} ln\left(\frac{W_1}{W_2}\right)$, (constant ρ, α) [4].

Where:
- η_p = propulsive efficiency
- γ_p = specific fuel consumption
- ρ = density of atmosphere
- S = wing reference area
- W_1 = initial weight
- W_2 = final weight

This means that Endurance is directly proportional to $C_L^{1.5}/C_D$, and Range is directly proportional to C_L/C_D. Hence, together, increasing C_L and decreasing C_D help improve endurance and range such that surveillance, reconnaissance and search and rescue missions can be more effective [5].

This paper aims to implement modifications on Delta wings for low-speed loitering flight by capitalising on its strong Leading-Edge Vortices (LEVs) developed over the wing. It will explore different design modifications adopted such as varying sweep angles, changing airfoil thickness and adding wing fences to maximise the lift generated by the LEVs through strengthening its core.

In reviewing past literature about sweep angle on Delta-winged planes, Brett and Ooi (2014) found that primary vortices was observed to detach from the leading edge, undergoing vortex breakdown for sweep angles of 50° and less, and resulted in reduced lift production near the wing tips loss of the stronger primary vortex [6]. However, this research only discussed an α of 10°, limiting the scope of the data collected and its relevance across different α.

Current literature by Birch and Dickens (2001) also shows that the highly swept-back configuration of the Delta wing with a large leading-edge sweep angle would encourage the airflow to span along the wingspan, contributing to lateral movement and the development of spanwise flow [7], worsened by low-speeds.

Additionally, in varying airfoil thickness-to-chord ratio from 2-15% for Delta wings at subsonic conditions with a sweep angle of 45°, Ghazijahani and Yavuz (2019) found that the increase of an airfoil thickness can reduce the LEVs in strength and delay the LEVs shedding [8].

Last, in consideration of the impact of wing fences, Ponnusamy et al. (2018) found that wing fences in swept wings are able to reduce induced drag by reducing spanwise flow [9]. Theoretically, this would help to increase C_L, enhancing range and endurance. However, the research is limited in that it was focused on swept, and not Delta wings.

Previous literature only discusses the effect of factors in isolation, but does not take into account how they may interact with one another to improve or worsen the achieved results. This study thus aims to compare the characteristics of Delta wings with and without modifications, as well as further understand the variations and interactions of the modifications implemented.

Materials and methods

The team kept the planform area fixed at 0.125 m^2 to stay under the 250g mass limit set by CAAS [10], and raised the sweep angle from 45° to 65° in 5° increments to balance feasibility of running tests and representativeness of results. Referring to the F-15SG RSAF design and other similar fighter jets as models, we took into consideration their shapes of modified cropped Delta wing shape with mostly 45° sweep angles- to establish key parameters like starting with a 45° sweep angle. The wingspan and root chord of aircrafts with the different sweep angles were then calculated. The NACA2412 airfoil was also selected for ease of construction when mounting the wing onto the fuselage, and ensuring predictable and well-understood behaviour as it is a widely used and thoroughly documented profile, with its aerodynamic characteristics extensively studied, [11]. The team chose a high wing configuration to allocate space within the fuselage for electronic components. Furthermore, the high wing configuration provides positive roll stability [12]. This design choice also ensures the structural integrity of the wing, as carbon spars can be seamlessly implemented throughout the entire wing structure without the need for breaking them. To ensure that the plane was structurally sound, fuselage width was determined from the width of electronics while the fuselage length was based on the root chord of the wing with 65° sweep, the longest root chord.

First, utilizing the equation $MAC = \frac{2}{3} \times Root\ chord \times \frac{1+\lambda+\lambda^2}{1+\lambda}$ for a delta wing, where Taper ratio = λ, MAC was calculated to be 23.6 cm for our plane. Then, taking reference from the recommendations in *Aircraft Design: A Conceptual Approach*, the position of the aerodynamic centre was assumed to be at the quarter chord point of the MAC [13], the vertical tail was sized to have a taper ratio of 0.4 [14], while the position of the tail ensured that the Tail Volume Coefficient remained around 0.04 [15]. The table below summarises key geometric and mass parameters for aircraft A1 after material was changed from 30 kg/m^3 instead of 52 kg/m^3 so that we could keep to the 250g weight limit set byCAAS [10]. Static margin was kept at 6%, which is a good amount for intermediates [16].

Parameter / Unit	Value
MAC of Delta wing / cm	23.6
Total Aircraft Mass / g	198.3
CG Distance / cm (from Nose Tip)	29.3
AC Distance / cm (from Nose Tip)	30.7
Position of Wing / cm (from Nose Tip)	47.3
Vertical Tail Distance / cm (from Nose Tip)	49.1

Table 1: Key Geometric and Mass Parameters A1

The team then decided to change our airfoil from NACA2412 to NACA2408 to facilitate the formation of more LEVs as thinner airfoils are known to have a sharper leading edge which promotes early separation of boundary layer and hence development of LEVs [17]. Based on preliminary CFD results, the team then decided to use an even thinner airfoil, replacing the NACA2408 airfoil with the NACA2404 to further enhance the generation of LEVs.

SolidWorks was used to design 8 types of modified Delta wings.

Model	A1	A2	A3	A4	A5	B	C1	C2
Planform area / m^2	0.125							
Airfoil	NACA2408					NACA2404		
Sweep angle / °	45	50	55	60	65	45	45	45
Wing fence position along span from fuselage / %	-	-	-	-	-	-	25	50

Table 2: Overview of Planes

ANSYS FLUENT student version was used to conduct CFD analysis. Freestream velocity was set at 10 m/s. Turbulent intensity of 1% was used. The k-epsilon turbulence model was chosen to investigate the aerodynamic characteristics of the wings under turbulent flow conditions. The maximum mesh count had to be kept within the 1,048,576 cell limit for the ANSYS FLUENT student version. Minimum and maximum mesh sizes also had to be repeatedly adjusted to adapt to fluent limitations, to ensure that the wings were also captured in the mesh.

Variable 1- Varying Sweep Angle from 45° - 65°

NACA2408 was initially chosen for ease of construction due to time and resource limitations. Delta A1 was the original baseline plane, a basic delta with a sweep angle of 45°.

Initial experimentations involved varying sweep angles across model A, as attached in Annex A (Figures A.2.1 to A.5.2).

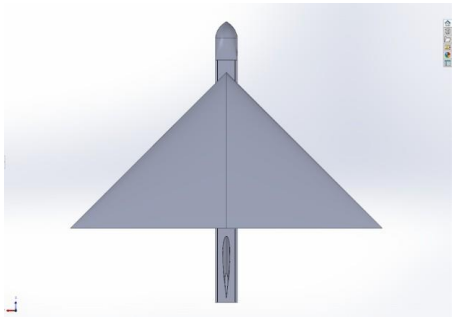

Figure 1: Top view of Delta A1

Variable 2 - Varying Airfoil Thickness

Attached in Annex A (Figures A.6.1 and A.6.2), Delta B is the first enhancement (2nd variable) to the prototype, utilising a thinner airfoil of NACA2404, created with the airfoil generator from Airfoil tools.

Variable 3 - Adding Wing Fences at 25% and 50% from Fuselage

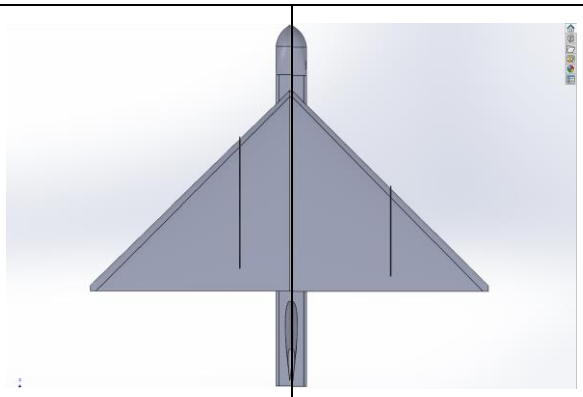

Figure 2:
Top view of Delta C1

Figure 3:
Top view of Delta C2

Delta C1 and C2 is the second enhancement to the prototype, with C1 having an additional wing fence ¼ of the wingspan away from the fuselage, and C2 having an additional wing fence at ½ of the wingspan. Model C builds upon the Delta B model, with an additional wing fence of thickness 1.25mm, with wing fence taking up 70% of the specific wing chord length. Other than thickness, remaining dimensions were scaled on the NACA2408 with a top protrusion of around 5 mm and a bottom protrusion of around 3 mm (Figure 4.1, 4.2).

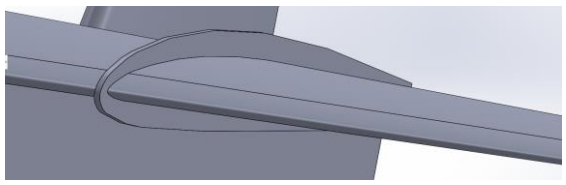

Figure 4.1: Wing fence for C1

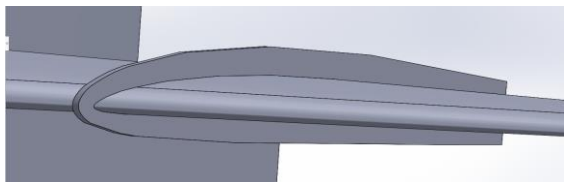

Figure 4.2: Wing fence for C2

Results

Delta model A (differing sweep angles)

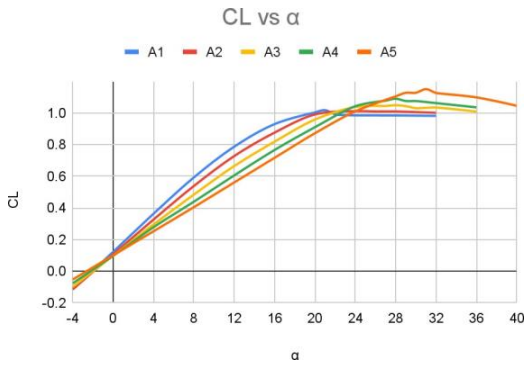

Figure 5.1: C_L vs α

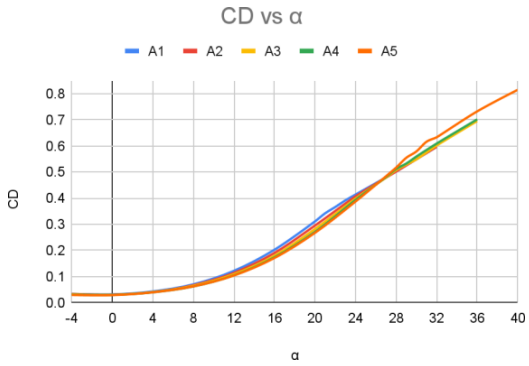

Figure 5.2: C_D vs α

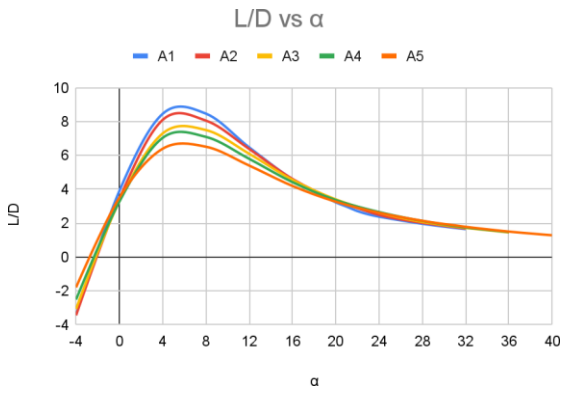

Figure 5.3: L/D ratio vs α

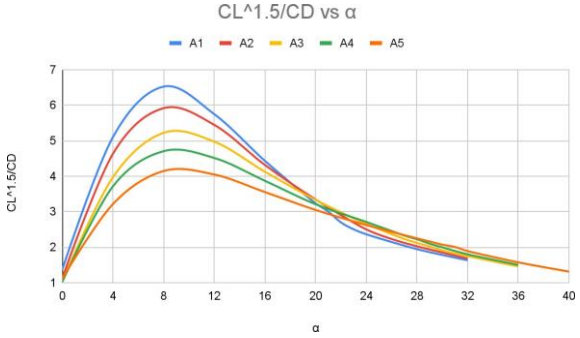

Figure 5.4: $C_L^{1.5}/C_D$ vs α

Comparing Delta model A1 vs Delta model B (NACA2408 airfoil vs NACA2404 airfoil)

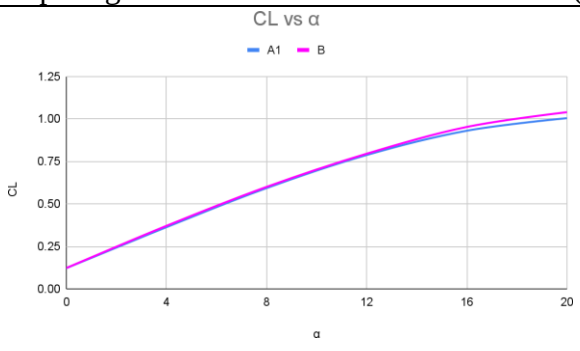

Figure 6.1: C_L vs α

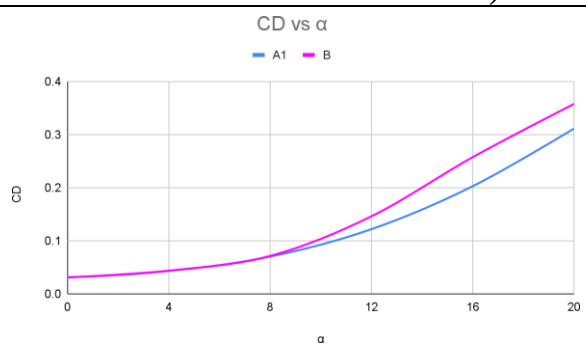

Figure 6.2: C_D vs α

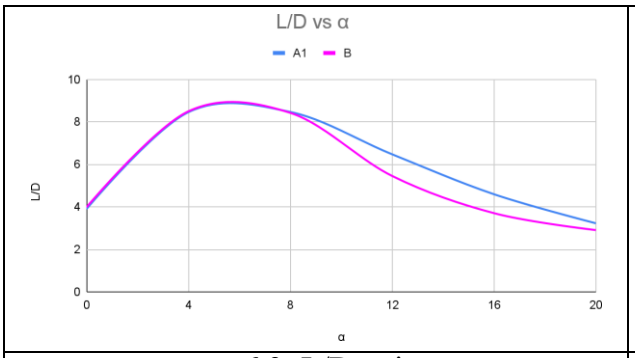

Figure 6.3: L/D ratio vs α

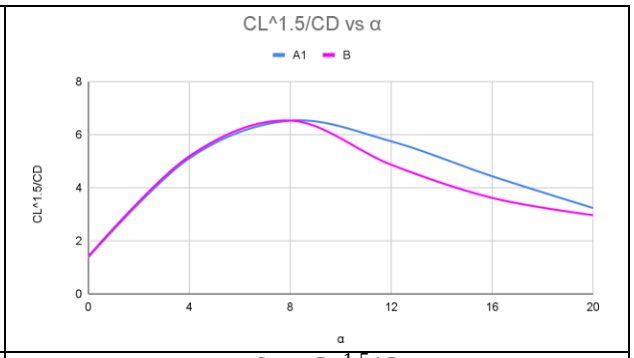

Figure 6.4: $C_L^{1.5}/C_D$ vs α

Comparing Delta model B vs Delta model C (Wing fences)

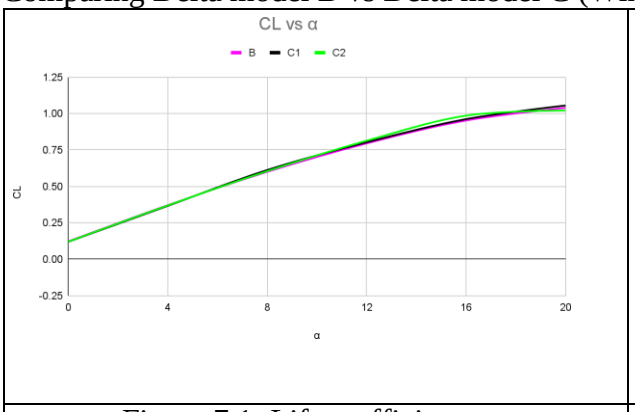

Figure 7.1: Lift coefficient vs α

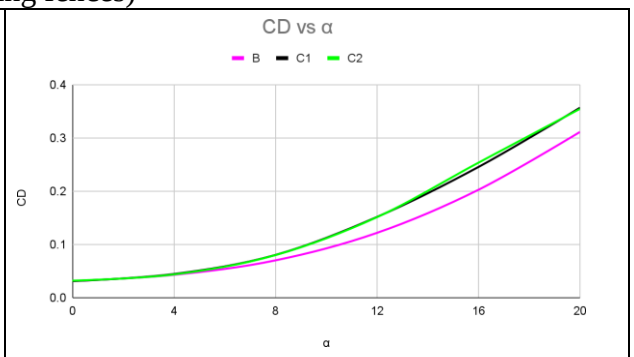

Figure 7.2: Drag coefficient vs α

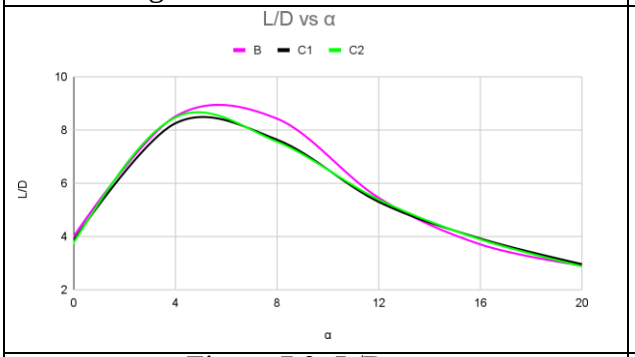

Figure 7.3: L/D vs α

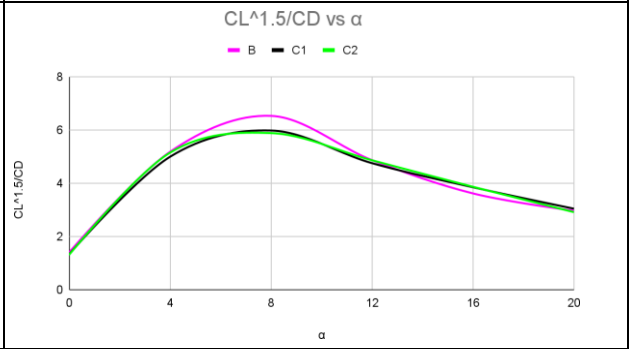

Figure 7.4: $C_L^{1.5}/C_D$ vs α

Discussion

Variable 1- Varying Sweep Angle from 45° - 65°

Regarding the first variable on sweep angles, Delta A2, A3, A4 and A5 all achieved higher $C_{L\ Max}$ values than Delta A1 due to its later stall, as shown in Figure 5.1, suggesting that higher maximum lift would be able to be achieved with higher sweep angles, causing the team to question if the increased formation of LEVs was seen in planes with higher sweep angles.

After experimenting with Ansys Student with the 3D Streamline simulation, it was then proven that highest LEVs were generated in Delta A5 at α of 16°, suggesting that the aforementioned hypothesis may be accurate. Although Delta A5 had the most LEVs, the number of LEVs formed was still much fewer than expected.

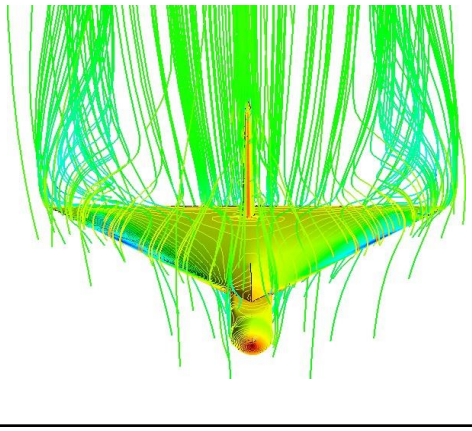

Fig 8.1: Air Flow on A5

However, upon closer examination of the graphs, Delta A1 had a much steeper gradient for the C_L vs α graph as compared to any of the other Delta A model planes. A steeper gradient signifies a larger increase in C_L with a change in α, meaning that a smaller α value is required to trim the aircraft. Additionally, from Figure 5.2, L/D vs α graph peaked at 6°, and was also the highest for A1. This means A1 is the most aerodynamically efficient among the 5 wings, with the point of efficiency maximised at 6°, resulting in maximised overall aerodynamic performance.

Variable 2- Varying Airfoil Thickness

The team hence decided to continue experimentation on the 45° sweep angle plane. To mitigate the issue of lack of LEVs, 2 methods were proposed. First, to use a thinner airfoil on the 45° sweep angle plane, and extrapolating the results for remaining model A planes. Second, to add additional vortex generators to increase flow separation and formation of LEVs. In approaching the problem, the team weighed the pros and cons, realising that a common issue faced during previous sweep angle CFD simulations was the inability to mesh small areas, which would have been worsened by option 2. Hence, the team chose option 1, which gave rise to model B (2nd variable).

CFD experiments revealed that Delta B achieved marginally higher lift C_L values (Figure 6.1), indicating the efficacy of thinner airfoils in generating more lift, attributed to the increased formation of LEVs due to increased low-pressure regions, as seen in Figure 8.2 and 8.3.

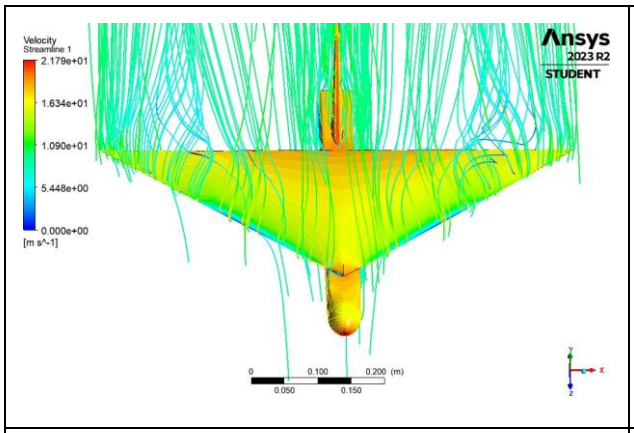

Figure 8.2: Airflow on A1

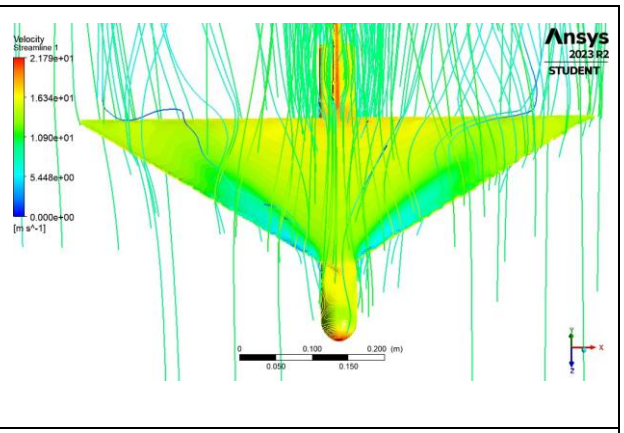

Figure 8.3: Airflow on B

However, C_D results, as seen in Figure 6.2, went against the team's initial hypothesis that the reduced surface area perpendicular to the airflow on Delta B would contribute to a lower $C_{D,k}$ thereby enhancing the overall L/D. Reduced airfoil thickness for low Reynolds number flow leads to earlier flow separation, resulting in an increase in drag and reduction in lift. However, reduction of airfoil thickness also enhances formation of LEVs, which might explain the increase

in lift at higher alpha values. A plausible explanation is that since velocity was set at a low value of 10m/s in our simulation, a low Reynolds' number for reduced airfoil thickness leads to earlier flow separation, resulting in increased drag and reduced lift. However, reduction of airfoil thickness also enhances formation of LEVs, which might explain the increase in lift at higher α values [18]. Ultimately, this also increases drag. As such, as seen from Figure 6.3, C_D increased by a greater extent than C_L, causing aerodynamic features of Delta B to ultimately be worsened, with a lower L/D ratio for Delta B than Delta A1.

Variable 3- Adding Wing Fences at 25% and 50% from Fuselage

From our CFD, one observation made was the large amount of spanwise flow seen in delta wings [7]. As such, a second modification was made to create model C – addition of wing fences (3rd variable). Wing fences act as barriers that help control the spanwise flow of air over the wings, as well as generate vortices outboard which result in increased suction on the wing surface beneath and higher C_L [19]. Despite existing literature mainly exploring wing fences in the context of swept wings rather than Delta wings [20], the team felt that this approach would be able to positively impact the aerodynamic characteristics of our Delta wing, and hence began exploring the approach.

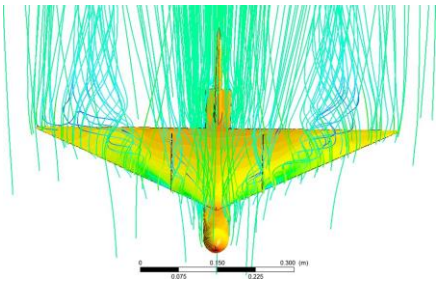

Figure 9.1: Airflow on C1

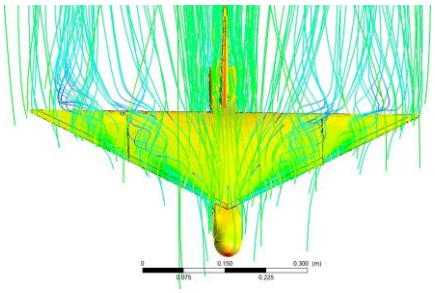

Figure 9.2: Airflow on C2

However, results went against our initial hypothesis. As seen from Figure 7.1 and 7.2, while C_L was marginally better in the C2 plane than C1 and B planes, which we attributed to the greater number of LEVs observed in the Delta wings with wing fences rather than the original Model B (NACA2404) plane, C_D appeared to be much higher for C1 and C2 than for model B. This suggests that while the wing fence at 50% of the wing best helps to limit spanwise flow, the more than proportional rise in C_D causes range and endurance to be negatively affected instead. (Figure 7.3 and 7.4)

Limitations

As stated previously, the CFD maximum mesh count size resulted in limitations during data collection. Despite being able to mesh the different configurations of the plane, more complex geometries like α of greater than 20° for model B required much more resources (roughly 2-3 million cells) for mesh to be successful in capturing both the fuselage and the wings. As such, the team was unable to collect these data, using instead values from 0° to 20° α as a basis for comparison. In doing so, we considered that low loitering flights often fly with low α, and hence deduced that data found would still be useful for extrapolation.

Conclusion

CFD analysis was conducted to determine the effect of changing the sweep angle, airfoil thickness and the addition of a wing fence on the aerodynamic characteristics of a Delta wing. It was found that the latter two modifications were able to strengthen LEVs and increase the overall C_L, despite L/D decreasing due to the larger increase in C_D.

Consequently, Delta A1 is still the best model to maximise loitering capability due to its higher endurance and range, and planes of similar configuration will be able to sustain low-speed loitering flight for a longer period of time. Hence, increasing sweep angle, making the airfoil thinner and adding wing fences would present negative effects on the overall performance, despite the strengthening of LEVs in models B and C, due to the excessive increase in drag.

Recommendations

Wing fences help to increase the LEVs observed on the plane, hence likely being able to produce more controllable lift, increasing the versatility of Delta-wing aircraft. Additionally, the simplicity of retro-fitting new wing fences into existing planes, such as the F-16 planes which are likely to be phased out in coming years as the nation transitions to F-35 planes [21], would enable the plane to be repurposed as a low-loitering aircraft, significant for a nation with few resources like Singapore.

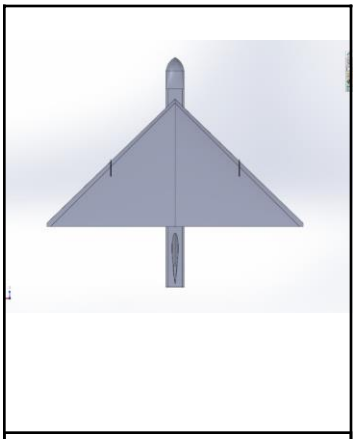

Figure 10: Top view of Proposed Delta

The team posits that the exploration of delta-wing aircraft performance in subsonic flight regimes, particularly with the integration of wing fences, is at a nascent stage and holds significant untapped potential. Advocating for an expanded research agenda, the team proposes a focused initiative to investigate the performance of non-uniform aircraft featuring varied wing fence positions and sizes under subsonic conditions. As seen from our research data, despite increased LEVs, disproportionate rise in C_D led to fall in L/D. Consequently, the team recommends a strategic reduction in the length of the wing fence, allowing for the continued harnessing of benefits while concurrently mitigating drag. This recommendation is firmly grounded in the conviction that such inquiries could yield substantial insights, contributing significantly to the advancement of knowledge in this domain, particularly given the limited research on wing fences in the context of Delta Wings.

Acknowledgements

The team would like to thank our mentors, Mr Jonathan Lim Zhi Wei and Mr Wong Jun Han Amos Timothy for their invaluable support and guidance through this research, as well as our teacher mentors Mr Alex Chang, Mdm Ang Wee Ling and Ms Wong Kai Ning for providing us guidance on our report. Additionally, the team would like to extend our sincere appreciation to Mr. Desmond Choong for his timely assistance in the workshop.

Bibliography

[1] Fuhrmann, M., & Horowitz, M. C. (2017). Droning on: Explaining the proliferation of unmanned aerial vehicles. International Organization, 71(2), 397–418. https://doi.org/10.1017/s0020818317000121

[2] Hitzel, S. M., Boelens, O. J., Rooij, M. and H¨ovelmann, A. (2016), 'Vortex development on the avt-183 diamond wing configuration – numerical and experimental findings', Aerospace Science and Technology 57, 90–102.

[3] Man-Vehicle Laboratory, MIT. (1997, March 16). *Theory of Flight*. Theory of flight. https://web.mit.edu/16.00/www/aec/flight.html

[4] Marchman, J. F., III. (2021, August 6). *Chapter 6. Range and Endurance*. Pressbooks. https://pressbooks.lib.vt.edu/aerodynamics/chapter/chapter-6-range-and-endurance/

[5] Marta, A., & Gamboa, P. (2014, September). Long Endurance Electric UAV for civilian surveillance missions. Long Endurance Electric UAV for Civilian Surveillance Missions. https://www.researchgate.net/publication/272162620_Long_Endurance_Electric_UAV_for_Civilian_Surveillance_Missions

[6] Brett, J., & Ooi, A. (2014). Effect of sweep angle on the vortical flow over Delta Wings at an α of 10 degrees. Journal of Engineering Science and Technology Vol. 9, No. 6 (2014) 768 - 781 . https://jestec.taylors.edu.my/Vol%209%20Issue%206%20December%2014/Volume%20(9)%20Issue%20(6)%20768-781.pdf

[7] Birch, J. M., & Dickinson, M. H. (2001, August 16). *Spanwise flow and the attachment of the leading-edge vortex on Insect Wings*. Nature News. https://www.nature.com/articles/35089071

[8] Ghazijahani, M. S., & Yavuz, M. M. (2019). Effect of thickness-to-chord ratio on aerodynamics of non-slender delta wing. *Aerospace Science and Technology*, *88*, 298–307. https://doi.org/10.1016/j.ast.2019.03.033

[9] Ponnusamy, V., Rajasekar, P. G., & Amman, K. B. (2018, December). A numerical investigation and optimization of Spanwise flow reduction using wing fence. International Journal of Mechanical and Production Engineering Research and Development (IJMPERD. https://www.researchgate.net/publication/330618013_A_NUMERICAL_INVESTIGATION_AND_OPTIMIZATION_OF_SPANWISE_FLOW_REDUCTION_USING_WING_FENCE

[10] CAAS. (n.d.). *UA Regulatory Requirements*. https://www.caas.gov.sg/public-passengers/unmanned-aircraft/ua-regulatory-requirements

[11] Matsson , O. J. E., Voth, J., McCain , C., & McGraw, C. (2016, June). Aerodynamicperformance of the NACA 2412 airfoil at low Reynolds number. ResearchGate. https://www.researchgate.net/publication/319271205_Aerodynamic_Performance_of_the_NAC A_2412_Airfoil_at_Low_Reynolds_Number
-

[12] Goodman, A. (1951, October 1). Effects of wing position and horizontal-tail position on the static stability characteristics of models with unswept and 45 deg sweptback surfaces with some reference to mutual interference. Defence Technical Information centre. https://apps.dtic.mil/sti/citations/ADA380548

[13] Raymer, D. P. (1989c). In Aircraft design: A conceptual approach (Second Edition, p. 50). essay, American Institute of Aeronautics and Astronautics.

[14] Raymer, D. P. (1989a). Airfoil and Geometry Selection. In Aircraft design: A conceptual approach (Second edition, pp. 55–57). essay, American Institute of Aeronautics and Astronautics, Inc., Washington, DC.

[15] Raymer, D. P. (1989b). Tail Volume coefficient. In Aircraft design: A conceptual approach (Second edition, pp. 110–113). essay, American Institute of Aeronauticals and Astronautics, Inc.,Washington, DC.

[16] Flying Wing CG Calculator. (n.d.). Rcplanes.online. Retrieved December 21, 2023, from https://rcplanes.online/cg_wing.htm#:~:text=Recommended%20Static%20Margin%3A

[17] Winslow, J., Otsuka, H., Govindarajan, B., & Chopra, I. (2017, December 15). *Basic understanding of airfoil characteristics at low Reynolds numbers* . Aerospace Research Central. https://arc.aiaa.org/doi/10.2514/1.C034415

[18] Sun, S., Kang, J., Lei, Z., Huang, Z., Si, H., & Wan, X. (2023, February 28). Analysis of the effect of the leading-edge vortex structure on unsteady secondary flow at the endwall of a high-lift low-pressure turbine. MDPI. https://doi.org/10.3390/aerospace10030237

[19] Whitford, R.(1987). *Design for Air Combat.* Jane's Information Group Limited

[20] Alam, M., Kara, K., & Alexander, A. (2022, June 20). Reduction of spanwise flow over a swept wing using an air curtain . Aerospace Research Central. https://arc.aiaa.org/doi/abs/10.2514/6.2022-3296

[21] Lim, M. Z. (2019, January 18). *F-35 fighter jets identified as "most suitable" to replace RSAF's f-16s: MINDEF*. The Straits Times. https://www.straitstimes.com/singapore/f-35-fighter-jets-identified-as-most-suitable-to-replace-rsafs-f-16s-mindef

Annex A

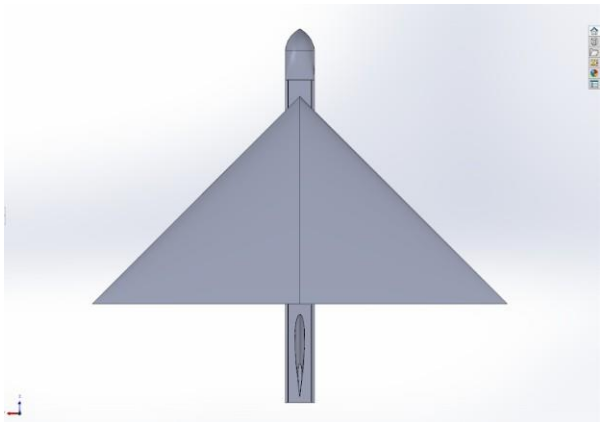

Figure A.1.1: Top view of Delta A1

Figure A.1.2: Side view of Delta A1

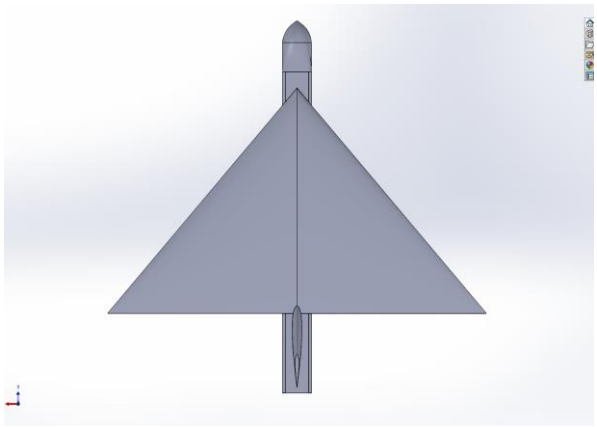

Figure A.2.1: Top view of Delta A2

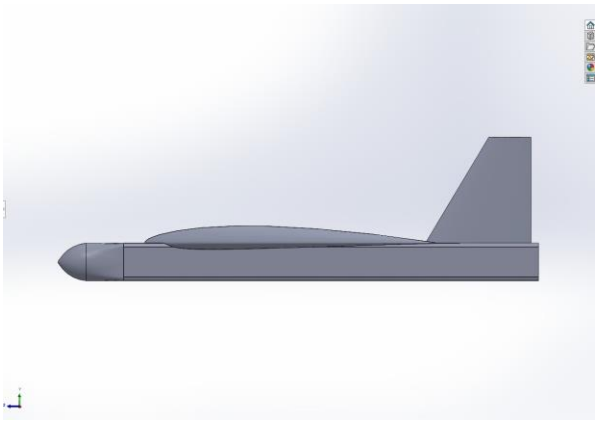

Figure A.2.2: Side view of Delta A2

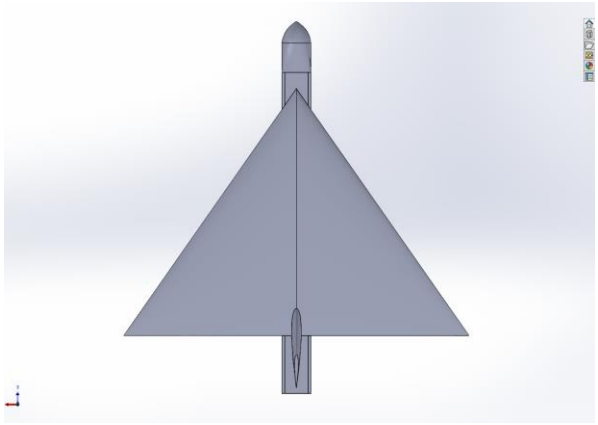

Figure A.3.1: Top view of Delta A3

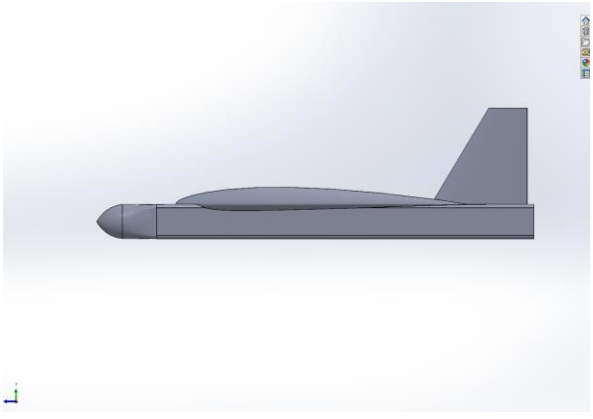

Figure A.3.2: Side view of Delta A3

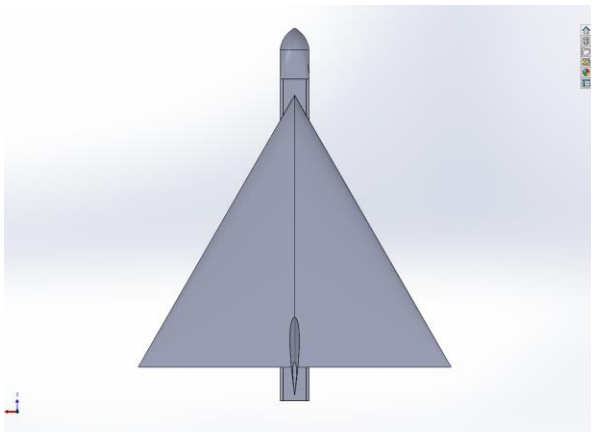

Figure A.4.1: Top view of Delta A4

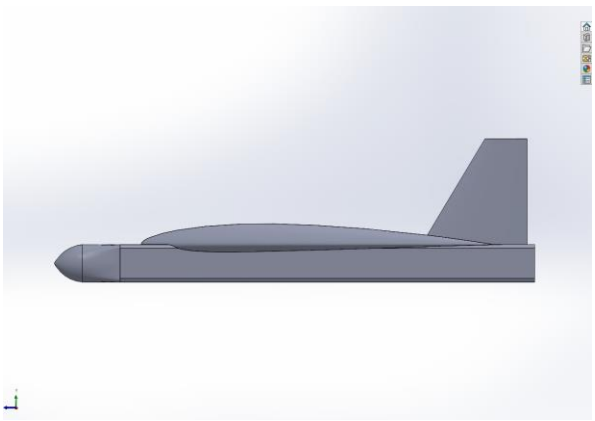

Figure A.4.2: Side view of Delta A4

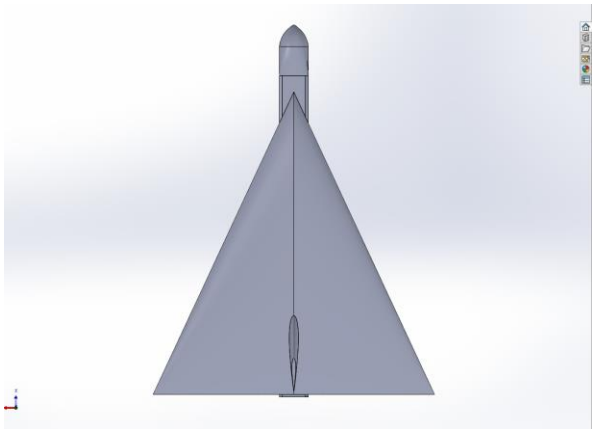

Figure A.5.1: Top view of Delta A5

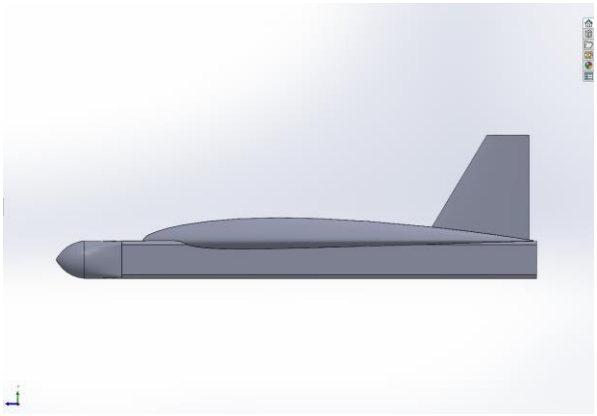

Figure A.5.2: Side view of Delta A5

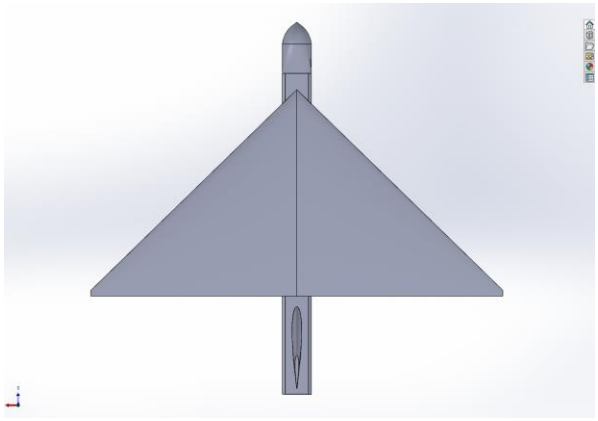

Figure A.6.1: Top view of Delta B

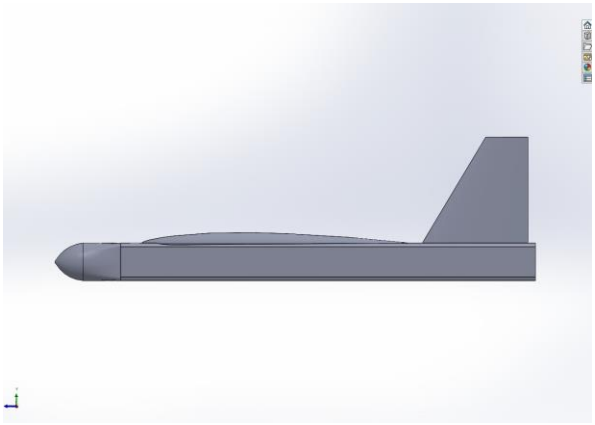

Figure A.6.2: Side view of Delta B

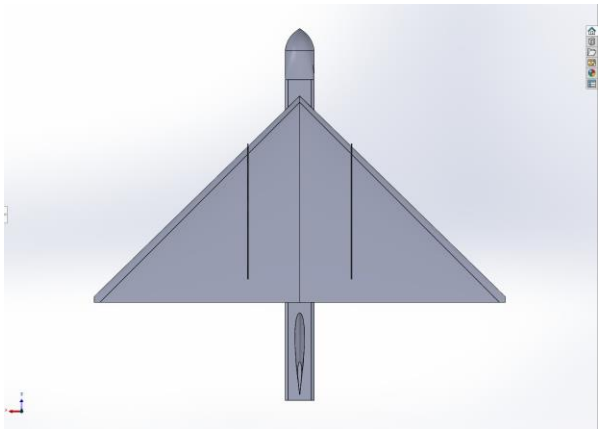	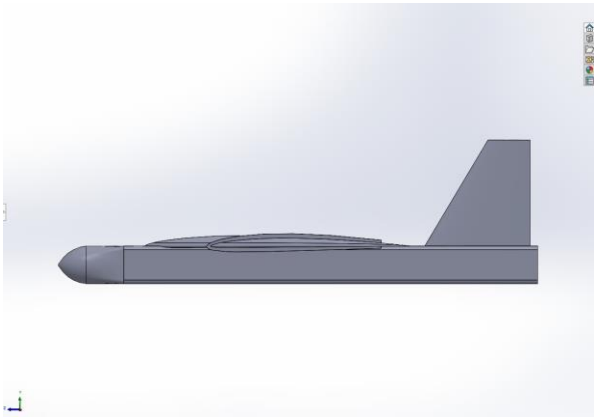
Figure A.7.1: Top view of Delta C1	Figure A.7.2: Side view of Delta C1
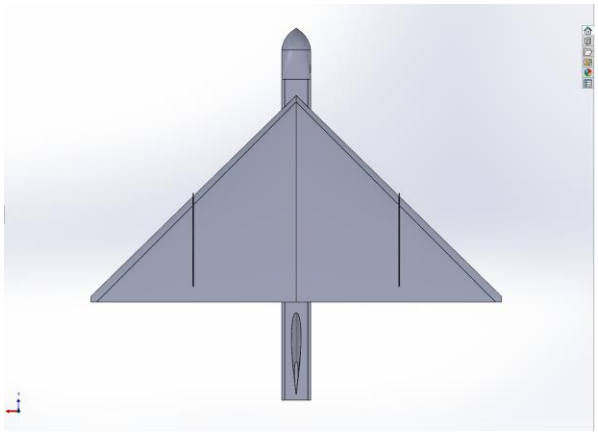	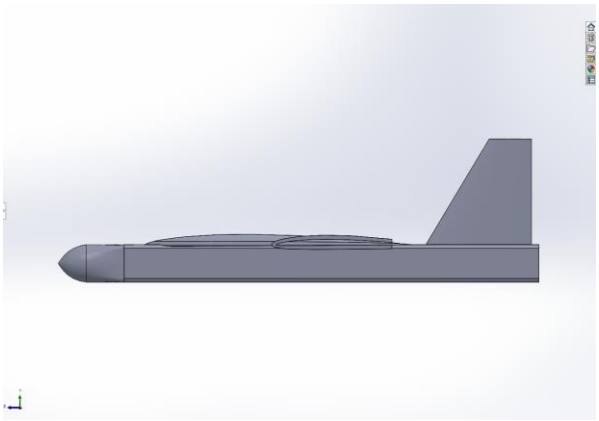
Figure A.8.1: Top view of Delta C2	Figure A.8.2: Side view of Delta C2

Annex B

A1 - 45° sweep, NACA2408

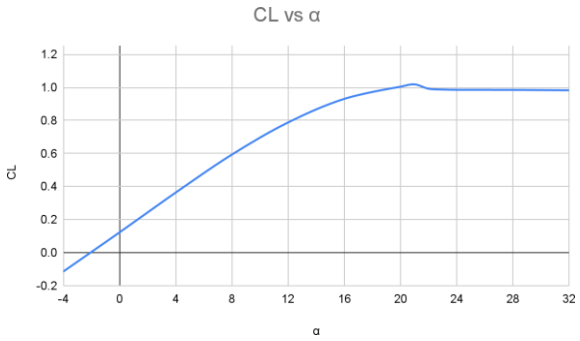

Figure B.1.1: C_L vs α

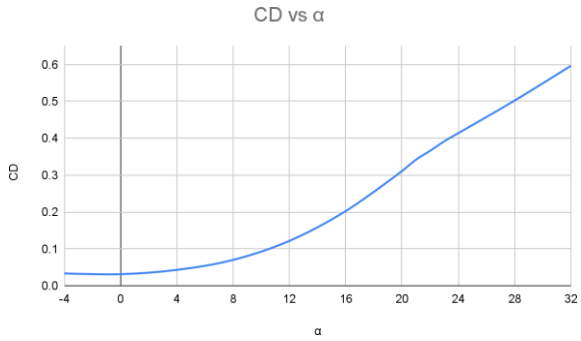

Figure B.1.2: C_D coefficient vs α

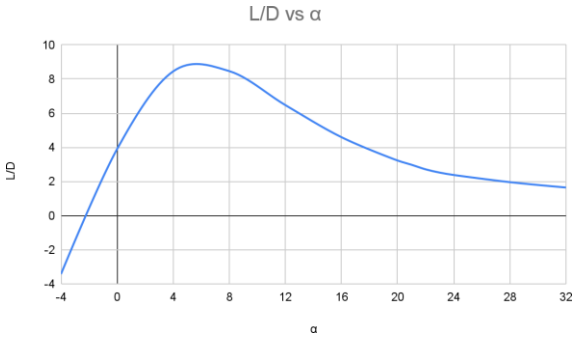

Figure B.1.3: L/D vs α

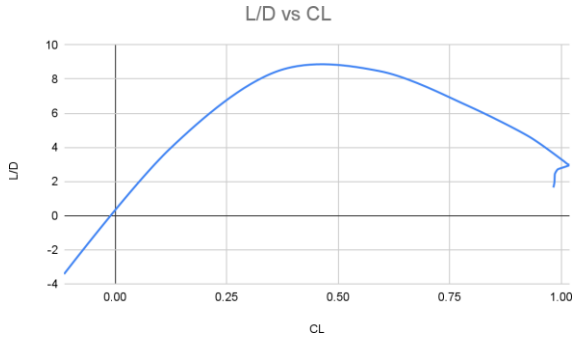

Figure B.1.4: L/D vs C_L

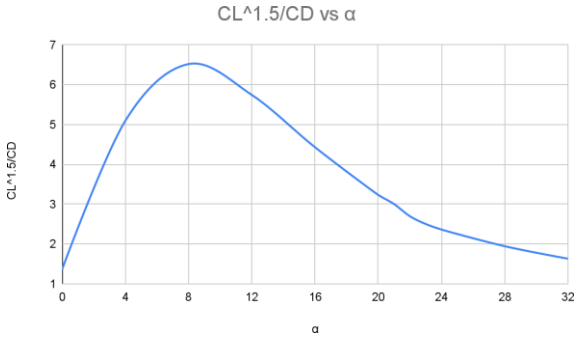

Figure B.1.5: $C_L^{1.5}/C_D$ vs α

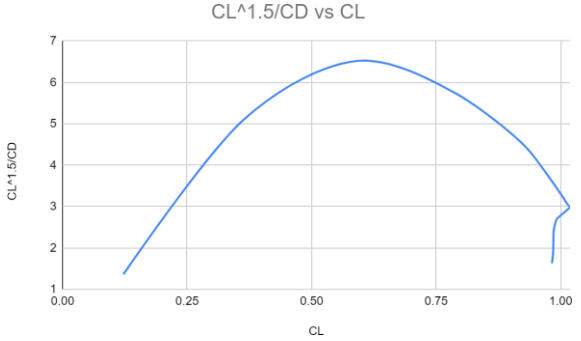

Figure B.1.6: $C_L^{1.5}/C_D$ vs C_L

A2 - 50° sweep, NACA2408

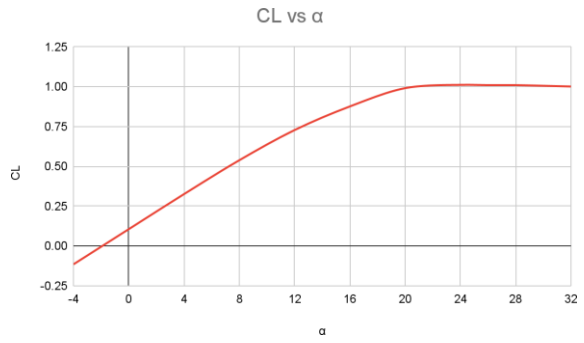

Figure B.2.1: C_L vs α

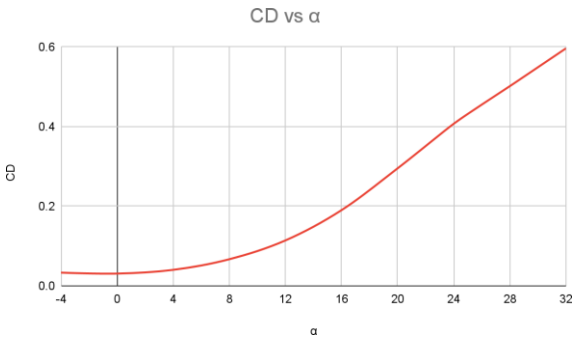

Figure B.2.2: C_D vs α

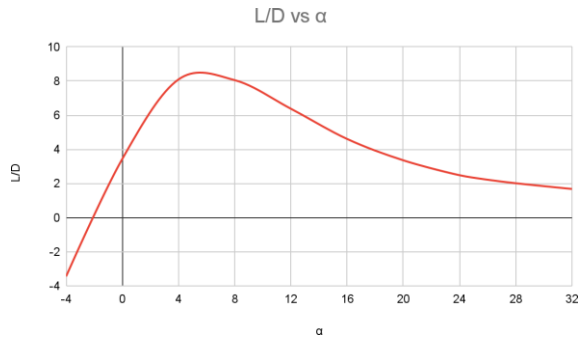

Figure B.2.3: L/D vs α

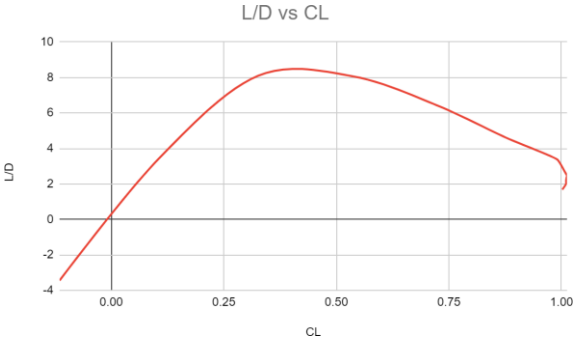

Figure B.2.4: L/D vs C_L

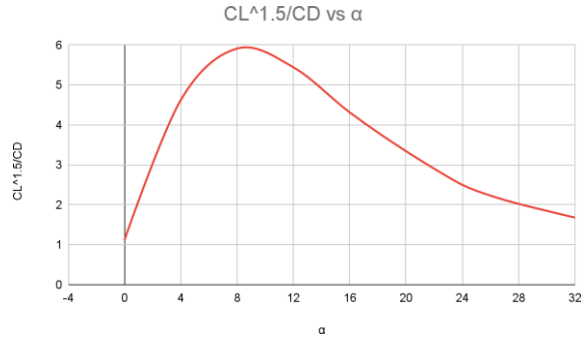

Figure B.2.5: $C_L^{1.5}/C_D$ vs α

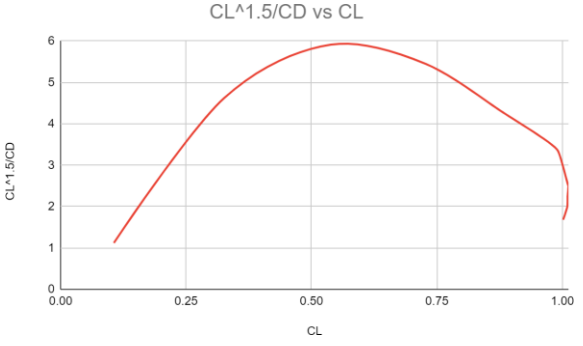

Figure B.2.6: $C_L^{1.5}/C_D$ vs C_L

A3 - 55° sweep, NACA2408

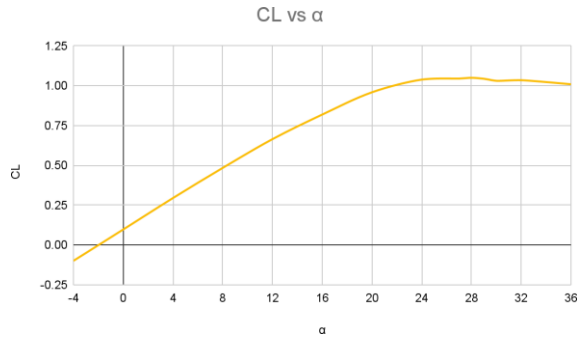

Figure B.3.1:C_L vs α

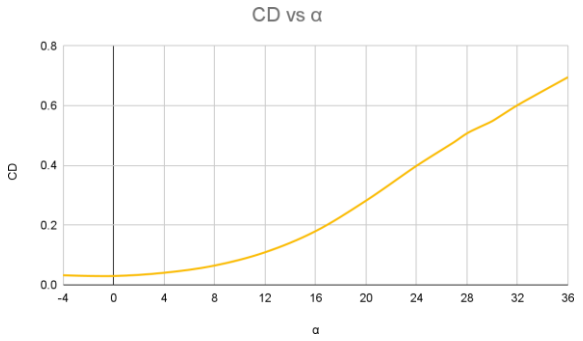

Figure B.3.2: C_D vs α

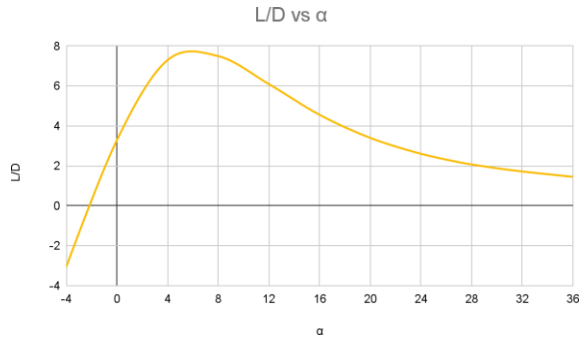

Figure B.3.3: L/D vs α

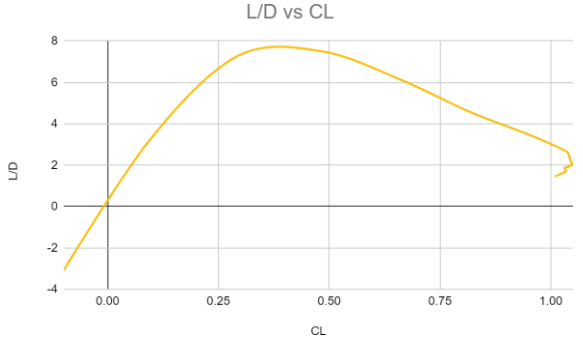

Figure B.3.4: L/D vs C_L

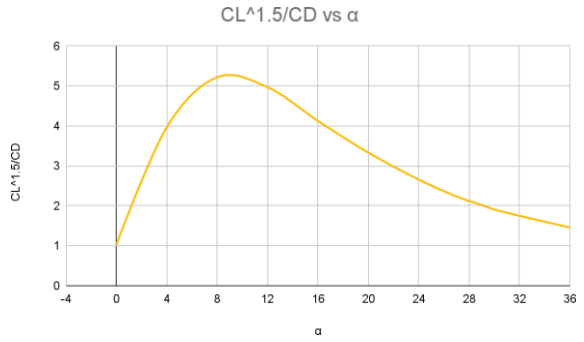

Figure B.3.5: $C_L^{1.5}/C_D$ vs α

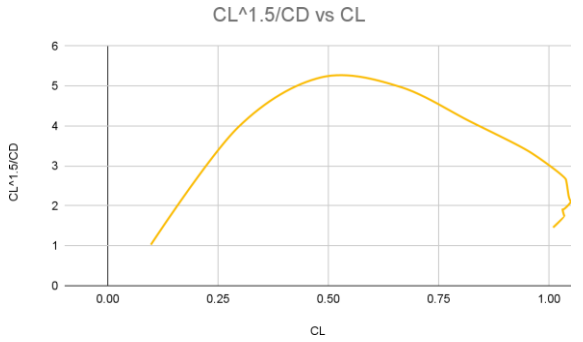

Figure B.3.6: $C_L^{1.5}/C_D$ vs C_L

A4 - 60° sweep, NACA2408

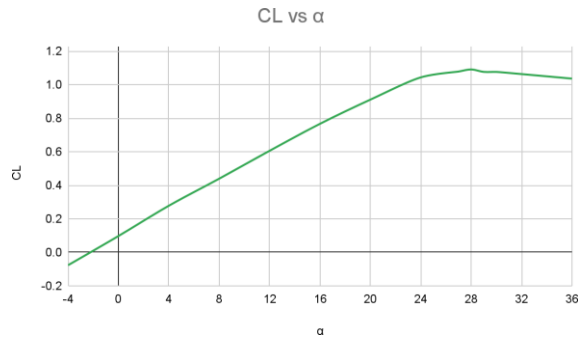

Figure B.4.1: C_L vs α

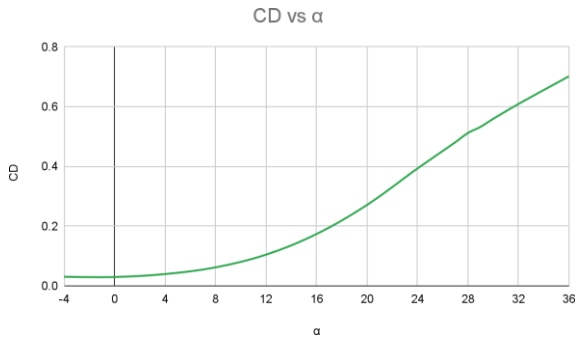

Figure B.4.2: C_D vs α

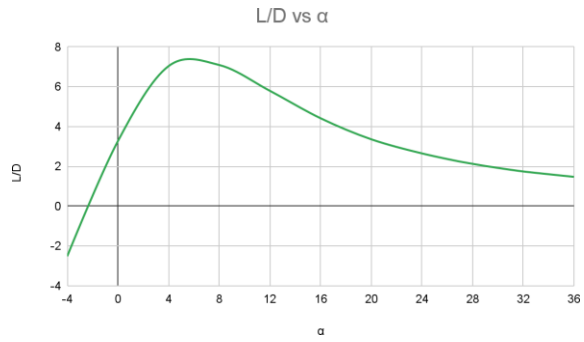

Figure B.4.3: L/D vs α

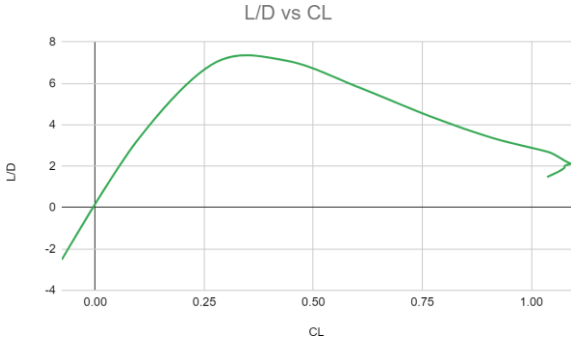

Figure B.4.4: L/D vs C_L

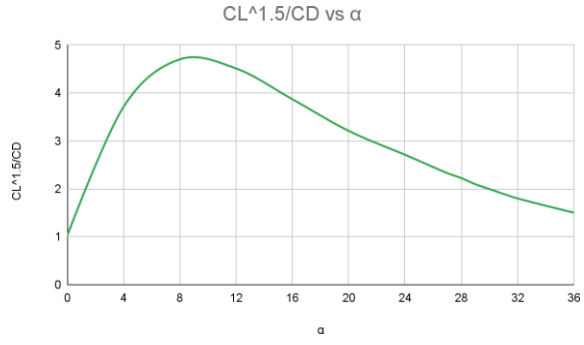

Figure B.4.5: $C_L^{1.5}/C_D$ vs α

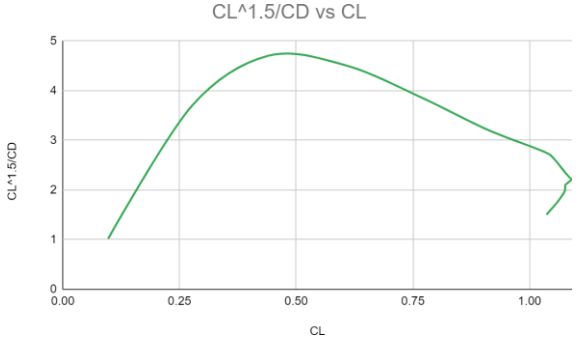

Figure B.4.6: $C_L^{1.5}/C_D$ vs C_L

A5 - 65° sweep, NACA2408

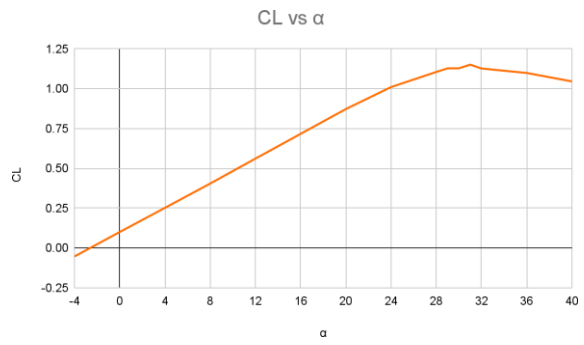

Figure B.5.1: C_L vs α

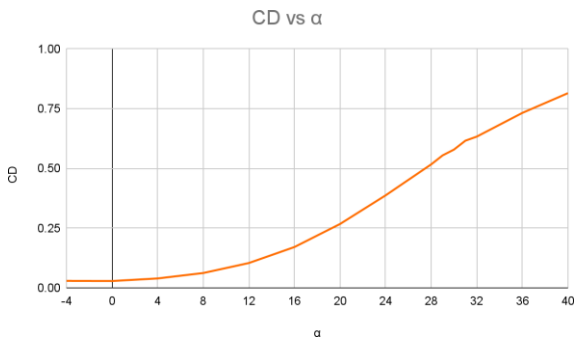

Figure B.5.2: C_D vs α

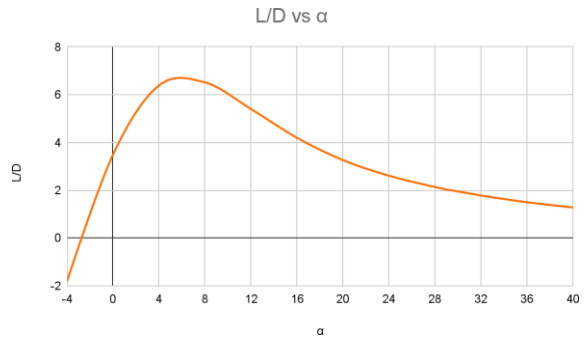

Figure B.5.3: L/D vs α

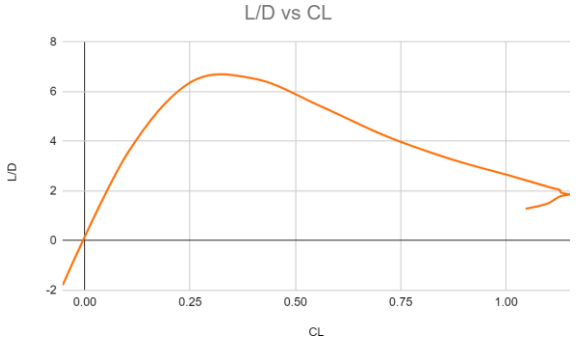

Figure B.5.4: L/D vs C_L

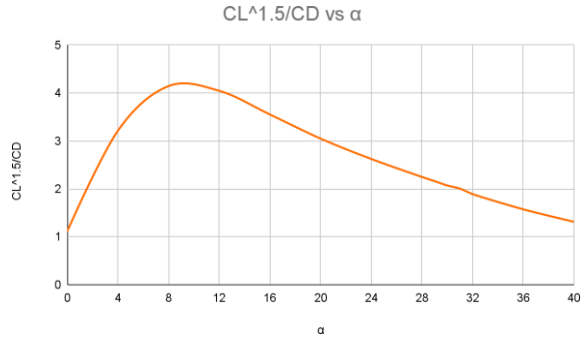

Figure B.5.5: $C_L^{1.5}/C_D$ vs α

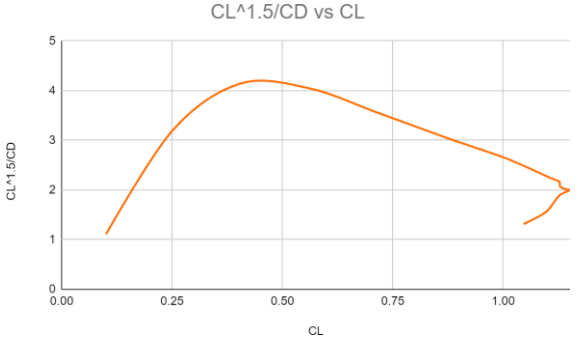

Figure B.5.6: $C_L^{1.5}/C_D$ vs C_L

Delta model A (differing sweep angles)

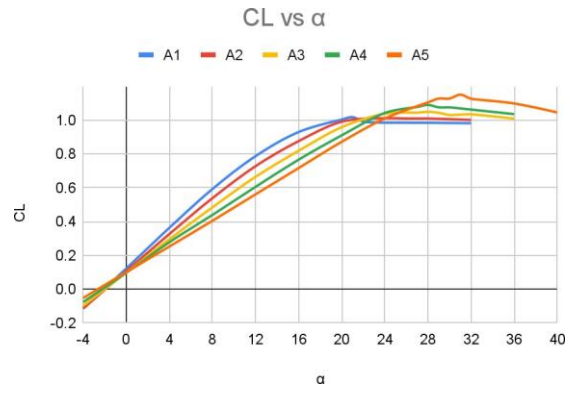

Figure B.6.1: C_L vs α

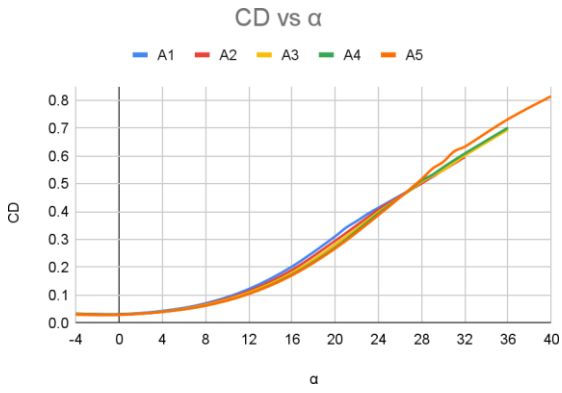

Figure B.6.2: C_D vs α

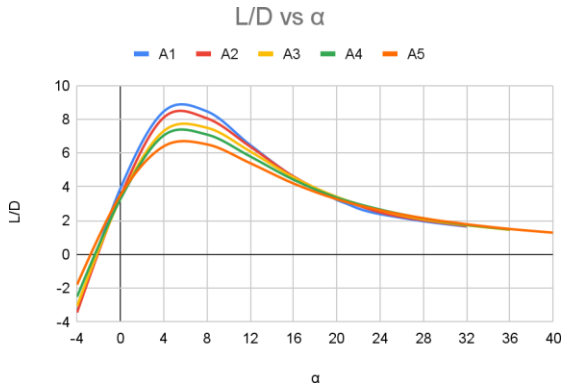

Figure B.6.3: L/D vs α

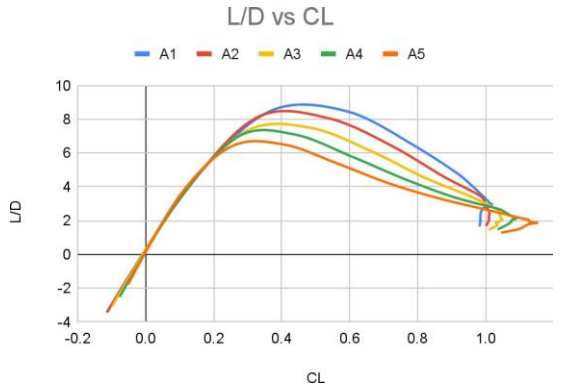

Figure B.6.4: L/D vs C_L

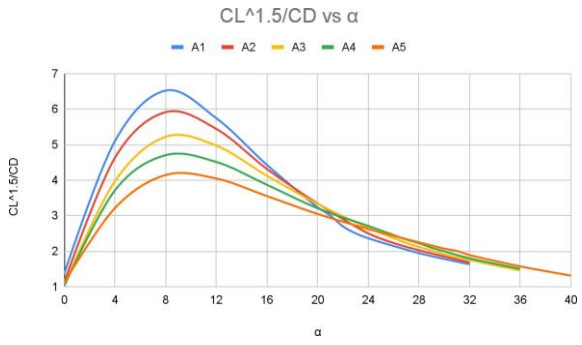

Figure B.6.5: $C_L^{1.5}/C_D$ vs α

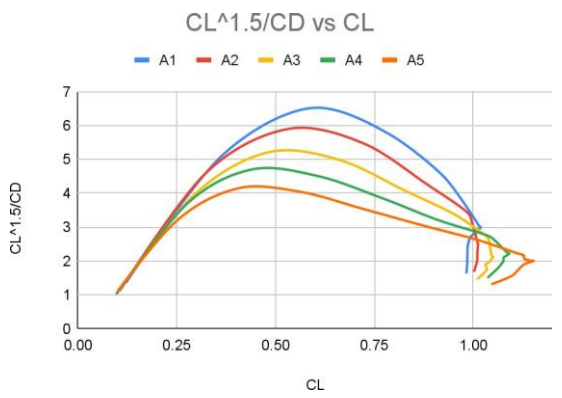

Figure B.6.6: $C_L^{1.5}/C_D$ vs C_L

B - 45° sweep, NACA2404

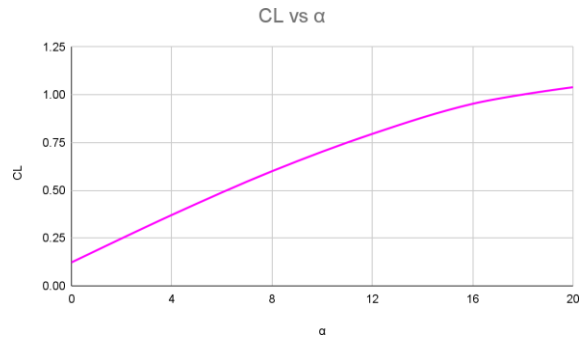

Figure B.7.1: C_L vs α

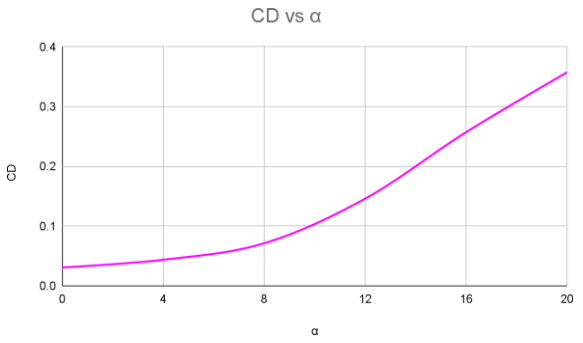

Figure B.7.2: C_D vs α

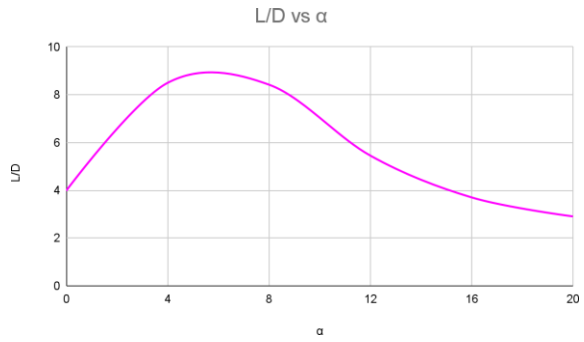

Figure B.7.3: L/D vs α

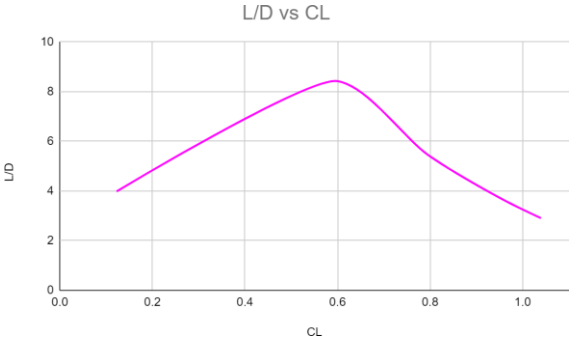

Figure B.7.4: L/D vs C_L

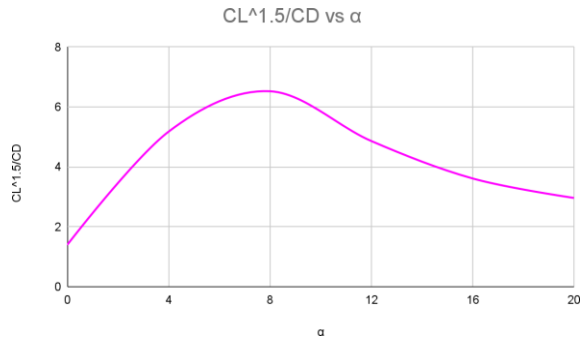

Figure B.7.5: $C_L^{1.5}/C_D$ vs α

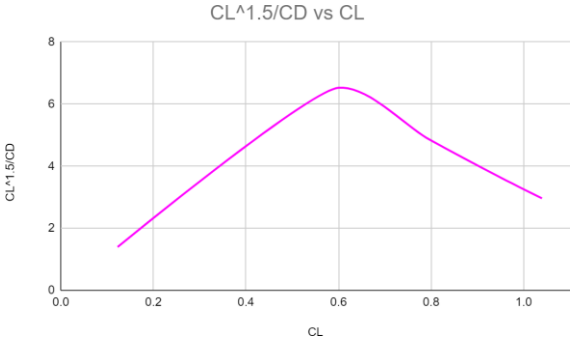

Figure B.7.6: $C_L^{1.5}/C_D$ vs C_L

Comparing Delta model A1 vs Delta model B (NACA2408 airfoil vs NACA2404 airfoil)

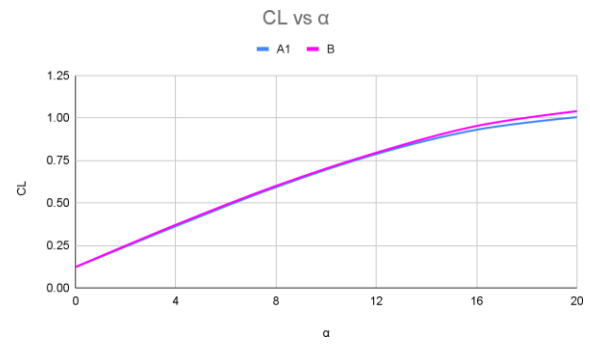

Figure B.8.1: C_L vs α

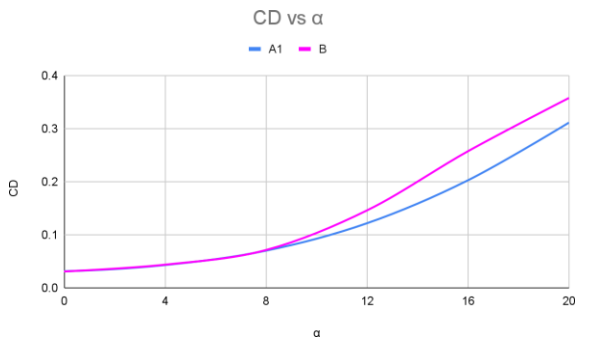

Figure B.8.2: C_D vs α

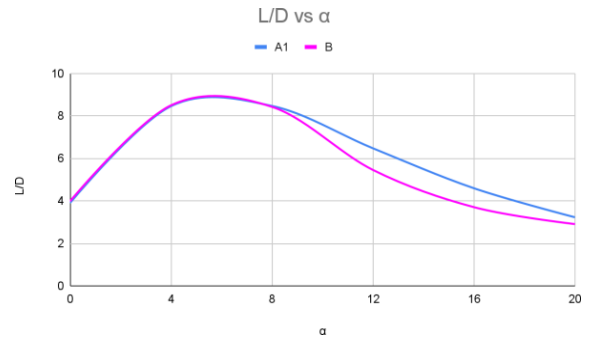

Figure B.8.3: L/D vs α

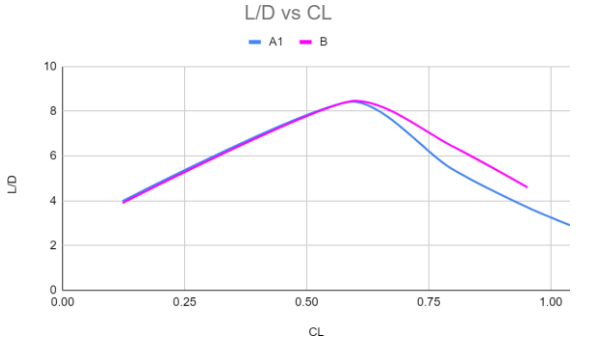

Figure B.8.4: L/D vs C_L

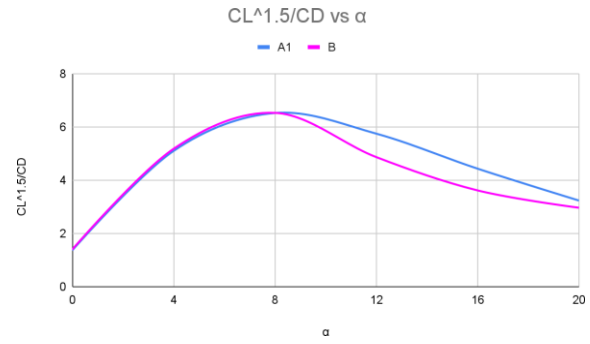

Figure B.8.5: $C_L^{1.5}/C_D$ vs α

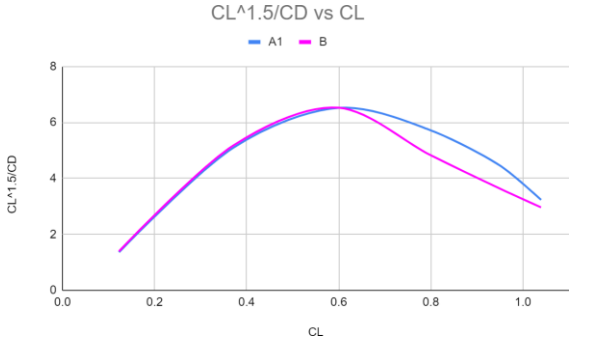

Figure B.8.6: $C_L^{1.5}/C_D$ vs C_L

C1 - 45° sweep, NACA2404, 25% wing fence

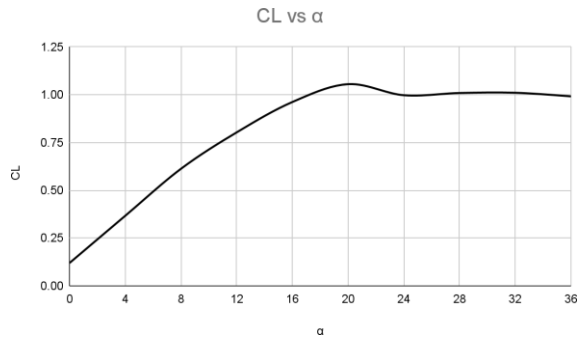

Figure B.9.1: C_L vs α

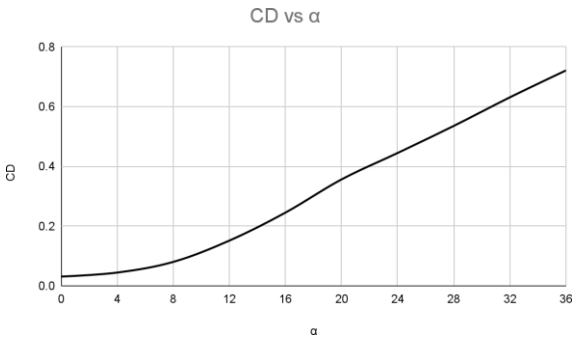

Figure B.9.2: C_D vs α

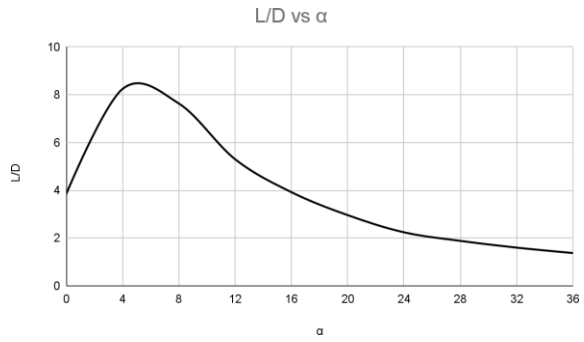

Figure B.9.3: L/D vs α

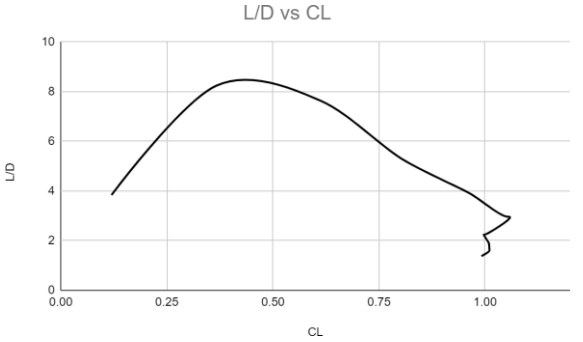

Figure B.9.4: L/D vs C_L

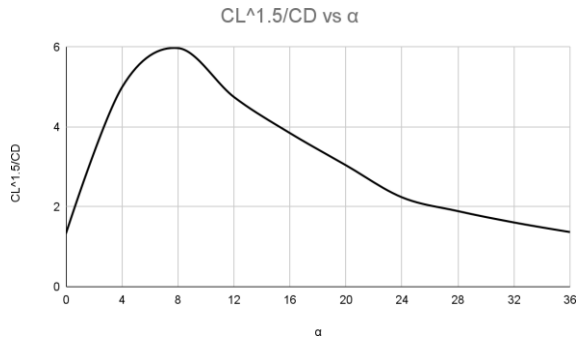

Figure B.9.5: $C_L^{1.5}/C_D$ vs α

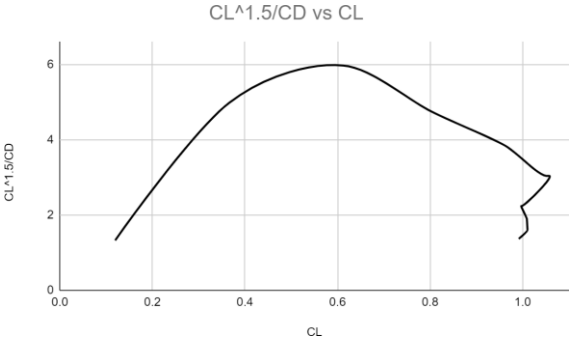

Figure B.9.6: $C_L^{1.5}/C_D$ vs C_L

C2 - 45° sweep, NACA2404, 50% wing fence

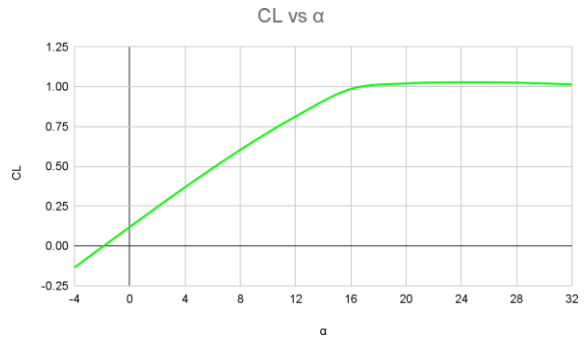

Figure B.10.1: C_L vs α

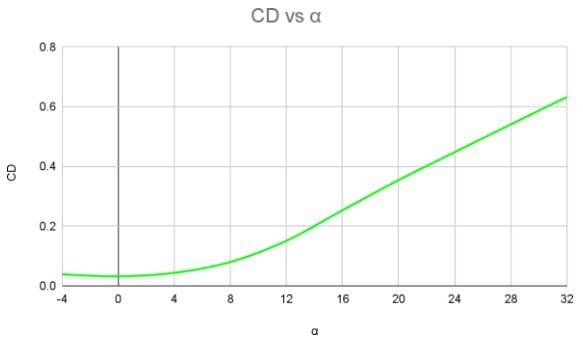

Figure B.10.2: C_D vs α

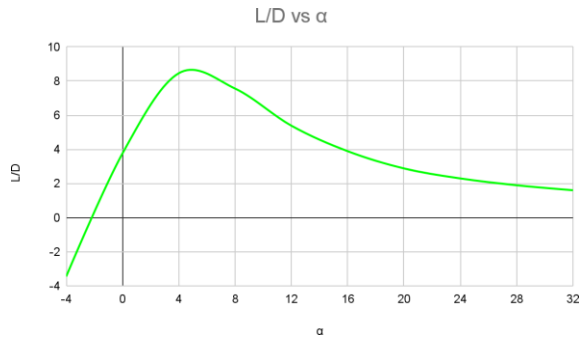

Figure B.10.3: L/D vs α

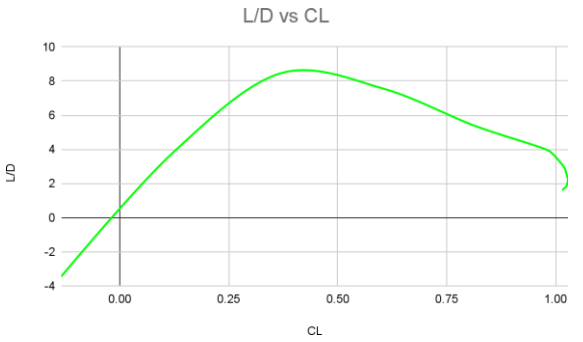

Figure B.10.4: L/D vs C_L

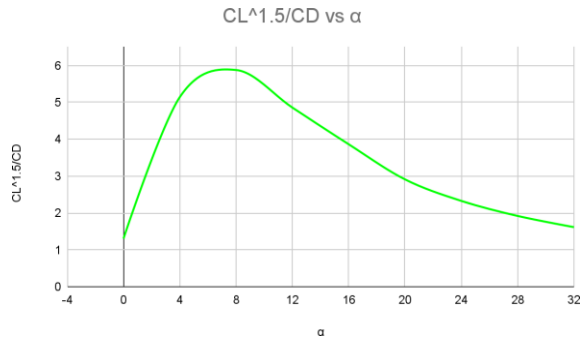

Figure B.10.5: $C_L^{1.5}/C_D$ vs α

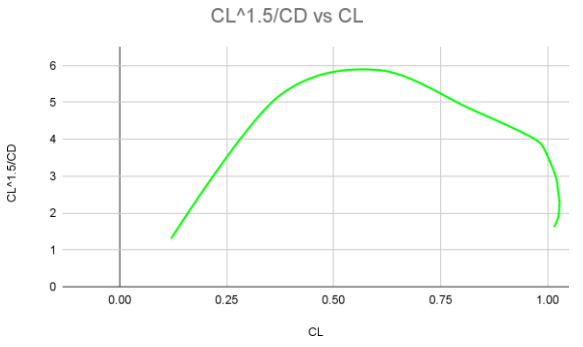

Figure B.10.6: $C_L^{1.5}/C_D$ vs C_L

Comparing Delta model B vs Delta model C (Wing fences)

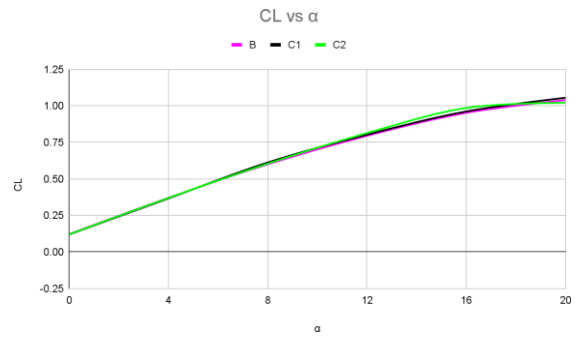

Figure B.11.1: C_L vs α

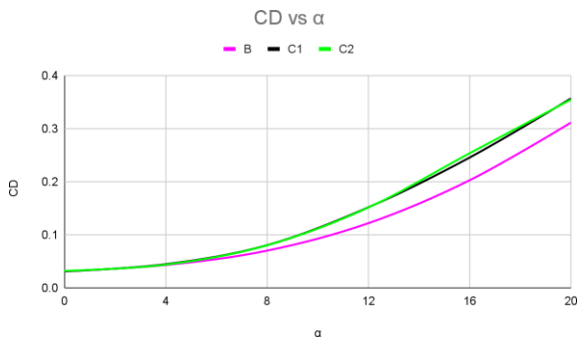

Figure B.11.2: C_D vs α

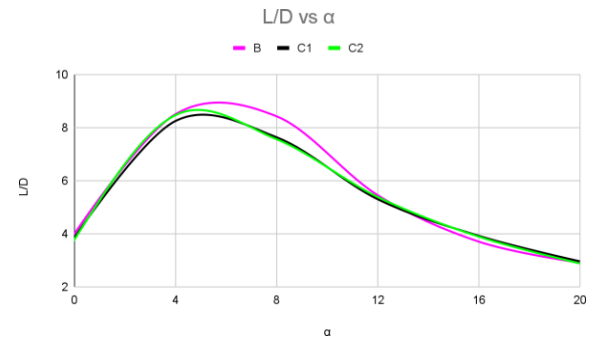

Figure B.11.3: L/D vs α

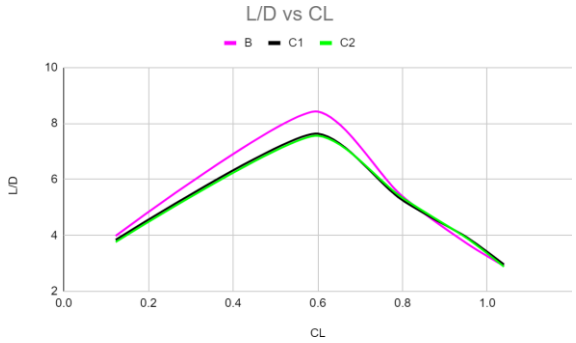

Figure B.11.4: L/D vs C_L

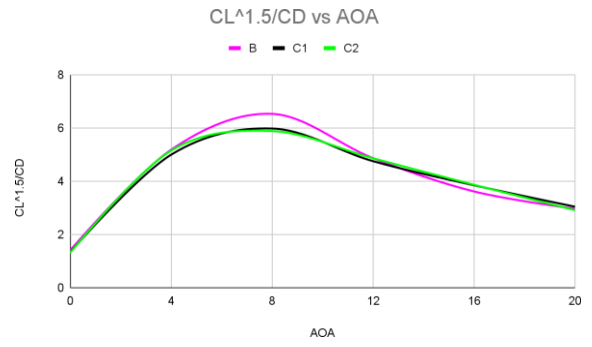

Figure B.11.5: $C_L^{1.5}/C_D$ vs α

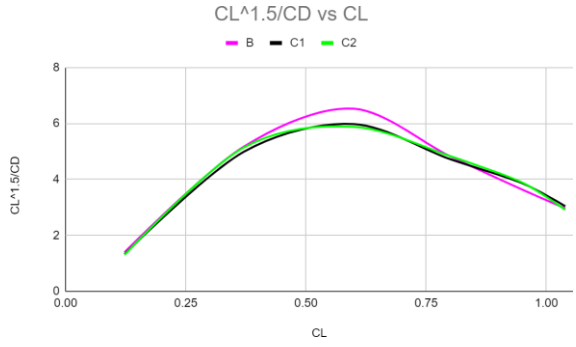

Figure B.11.6: $C_L^{1.5}/C_D$ vs C_L